

^{48}Ca -induced reaction on the lanthanide target ^{154}Gd and its decay to ground and metastable states within the dynamical cluster-decay model

Pooja Kaushal, Arshdeep Kaur,* Hemdeep, Sahila Chopra, and Raj K. Gupta
Department of Physics, Panjab University, Chandigarh 160014, India

 (Received 3 May 2018; published 3 July 2018)

The decay mechanism of compound nucleus (CN) $^{202}\text{Po}^*$, formed in $^{48}\text{Ca} + ^{154}\text{Gd}$ reaction, is studied within the dynamical cluster-decay model (DCM) at various excitation energies E_{CN}^* , where neutron emission xn , $x = 3-5$, are the predominant decay modes. The study is of interest since $^{202}\text{Po}^*$ decays to the ground state (g.s.) of ^{198}Po by emission of $4n$ and to metastable states ^{199m}Po and ^{197m}Po via $(3n, 5n)$ emission, respectively. The DCM is applied here for the first time to the decays of metastable states. Both types of decays are analyzed separately, using neck-length ΔR (equivalently, barrier-lowering) parameter, the only parameter in the DCM, to best fit the evaporation residue or channel cross section (σ_{xn}) data and predict the quasifissionlike (qf-like) noncompound (σ_{qf}) and fusion-fission (σ_{ff}) cross sections. For g.s. to g.s. decay of $^{202}\text{Po}^*$, possibly due to involving the deformed rare-earth lanthanide target ^{154}Gd , the observed $4n$ decay channel requires the noncompound nucleus (nCN) contribution, treated as the qf-like process. On the other hand, the decay mechanism of $^{202}\text{Po}^*$ to metastable states (m.s.) ^{199m}Po and ^{197m}Po , is a pure CN decay, i.e., the σ_{qf} is zero. In this study, we have included the deformation effects up to quadrupole deformations β_{2i} and optimum orientations θ_i^{opt} for coplanar ($\Phi = 0^\circ$) nuclei, using hot-compact configurations, supporting asymmetric fission of CN $^{202}\text{Po}^*$. The variation of CN formation probability P_{CN} and survival probability P_{surv} with excitation energy E_{CN}^* is in complete agreement with the known systematic of other radioactive CN studied so far, thereby giving credence to the predicted σ_{qf} in g.s. to g.s. decay and fusion-fission cross section σ_{ff} of $^{202}\text{Po}^*$. Interestingly, both the observed g.s. to g.s. and g.s. to m.s. processes occur at a fixed $\Delta R = 2.45 \pm 0.20$ fm, which is within the nuclear proximity limit of ~ 2.5 fm, and hence useful for making predictions.

DOI: [10.1103/PhysRevC.98.014602](https://doi.org/10.1103/PhysRevC.98.014602)

I. INTRODUCTION

The doubly magic ^{48}Ca -induced reactions on strongly deformed actinides Th to Cf, synthesizing superheavy elements $Z = 110-118$, are the well-known warm fusion reactions, observed with $3n$, $4n$ emissions (in between the cold and hot fusion with $1n, 2n$ and $4n, 5n$ emissions, respectively), the so-called evaporation residues (ERs), fusion-fission (ff), and quasifission (qf) decay products [1,2]. Similarly, ^{48}Ca -induced reactions on strongly deformed lanthanide targets Sm to Yb from the rare-earth region [3-8] forming CN Pb* to Th* are also expected [6-10] to decay via qf-like noncompound nucleus (nCN) decay, though not yet explicitly measured experimentally (the equivalent fusion suppression is observed for the reaction with the deformed target, showing no such evidence for the corresponding spherical target [6,7]). Theoretically, for the compound nucleus (CN) $^{220}\text{Th}^*$, the analysis of experimental data by Hinde *et al.* [9] as well as the dynamical cluster-decay model (DCM) calculation of our group [10] show that the qf-like nCN effects are clearly present in such reactions. The experimental data on the use of strongly deformed rare-earth targets exist for various entrance channel heavy-ion reactions $^{40}\text{Ar} + ^{180}\text{Hf}$ [3,4] and $^{48}\text{Ca} + ^{172}\text{Yb}$ [5], both forming the

strongly fissioning $^{220}\text{Th}^*$ CN, and other ^{48}Ca -based reactions on $^{144,154}\text{Sm}$ [7] and ^{154}Gd , ^{159}Tb , ^{162}Dy , and ^{165}Ho [8], and $^{168,170}\text{Er}$ [6] also forming strongly fissioning radioactive CN $^{192,202}\text{Pb}^*$, $^{202}\text{Po}^*$, $^{207}\text{At}^*$, $^{210}\text{Rn}^*$, $^{213}\text{Fr}^*$, and $^{216,218}\text{Ra}^*$. In this paper, we concentrate on $^{48}\text{Ca} + ^{154}\text{Gd} \rightarrow ^{202}\text{Po}^*$, which is observed [8] to decay not only via the ground state (g.s.) to ground state but also from g.s. to (excited) metastable (m.s.) states.

The entrance channel properties, in particular, the entrance channel mass asymmetry and the deformation of at least one of the colliding nucleus [7] seem to play an important role in the reaction dynamics of qf. Also, for systems with large entrance channel Coulomb repulsion $Z_p Z_t$, Z_p and Z_t being the proton number of projectile-target pair, the fusion hinderance (equivalently nCN process) is expected to contribute significantly [11]. Specifically, various projectiles (^{16}O , ^{24}Mg , ^{34}S , and ^{48}Ti) on different rare-earth targets forming CN $^{202}\text{Po}^*$ [11] show that the fusion hinderance or the nCN process is expected to become important for $Z_p Z_t \gtrsim 1000$. It is interesting to note that our choice of $^{48}\text{Ca} + ^{154}\text{Gd}$ reaction is of fairly asymmetric target-projectile combination, with deformed target ^{154}Gd and $Z_p Z_t = 1280$.

For ^{48}Ca beam on ^{154}Gd target at various laboratory energies $E_{\text{lab}} = 185-201.5$ MeV [8], the experimental data is available only for evaporation residue (ER) cross sections of $^{202}\text{Po}^*$ that decay predominantly by x neutrons (xn), $x = 3-5$, emission. The $^{202}\text{Po}^*$ decays to ground state of ^{198}Po by emission of $4n$ and to metastable states ^{199m}Po and ^{197m}Po , respectively,

*Present address: Sri Guru Gobind Singh College, Sector 26, Chandigarh, India.

by $3n$ and $5n$ emissions, with metastable excitation energies $\varepsilon = 0.310$ and 0.204 MeV [12], both above their respective ground states. The model used here to analyze this reaction is the dynamical cluster-decay model (DCM) [13–19], which is based on the quantum mechanical fragmentation theory (QMFT), and includes the deformation and orientation effects of the incoming nuclei or outgoing decay fragments. Our calculations here for both the g.s. to g.s. and g.s. to m.s. decays, are made for quadrupole (β_{2i} ; $i = 1, 2$) deformations with optimum orientations (θ_i^{opt}) of the coplanar nuclei, i.e., two nuclei or fragments lying in the same plane ($\Phi = 0^\circ$), using hot-compact configurations, which have the highest interaction barriers and the smallest interaction radii [16], supporting asymmetric fission of $^{202}\text{Po}^*$, as is also indicated for the decay of neighboring $^{204}\text{Po}^*$ [17] and other radioactive CN such as $^{220}\text{Th}^*$ [10]. Within the DCM, the decay to (excited) metastable states is analyzed here for the first time.

The only parameter of the DCM is the neck-length ΔR , used to best fit the observed ER cross section σ_{ER} ($= \sigma_{4n}$ in g.s. to g.s. decay, and $= \sum \sigma_{xn}$, $x = 3, 5$ for g.s. to m.s. decays) or the channel cross sections σ_{xn} itself, and allow us to predict the fusion-fission cross section σ_{ff} and quasifissionlike nCN cross section σ_{qf} . The ΔR value for a particular decay channel refers to the reaction time scale for that channel.

Note that the DCM is a nonstatistical quantum-mechanical model used to study the decay of hot and rotating CN at low excitation energy. On the other hand, as an alternative, many other theoretical groups use the statistical models to perform similar analysis to the present one, and there is enough important literature on this model [4, 8, 20–24]. One such calculation for $^{202}\text{Po}^*$ CN studied here exists [8] on the basis of the statistical model, where $\sigma_{\text{fusion}} (\equiv \sigma_{\text{capture}})$ was estimated by using the diffused barrier formula from the fusion by diffusion model of Świątecki *et al.* [22], the CN fusion probability by using a phenomenological expression of Siwek-Wilczyńska *et al.* [23], and the CN survival probability according to the formula of Vandenbosch and Huizenga [24], derived from transition-state theory, whose results are compared here with the present DCM calculations (refer to Fig. 7).

The paper is organized as follows. A brief description of the QMFT-based DCM for hot and rotating compound nuclei is given in Sec. II. Our calculations and results of (i) g.s. to g.s. decay of $^{202}\text{Po}^*$ to ^{198}Po , formed in $^{48}\text{Ca} + ^{154}\text{Gd}$ reaction, and (ii) the decay of $^{202}\text{Po}^*$ in g.s. to m.s. ^{199m}Po and ^{197m}Po are discussed in Sec. III. Finally, a summary of our results is given in Sec. IV. A first report of this work was presented in Ref. [25].

II. DYNAMICAL CLUSTER-DECAY MODEL (DCM)

DCM is a nonstatistical model used to understand the decay of hot and rotating CN formed in low-energy heavy-ion reactions. The model is based on the dynamical or quantum-mechanical fragmentation theory [13–15] in which the decay of a hot CN with temperature T and angular momentum ℓ , is worked out in terms of the collective coordinates of mass (and charge) asymmetries $\eta = (A_1 - A_2)/(A_1 + A_2)$ [and $\eta_Z = (Z_1 - Z_2)/(Z_1 + Z_2)$] and relative separation coordinate R , multipole deformations $\beta_{\lambda i}$ ($\lambda = 2, 3, 4$; $i = 1, 2$), orientations

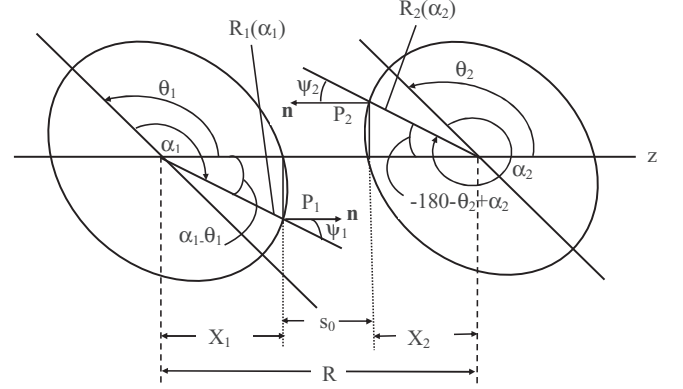


FIG. 1. Schematic configuration of two equal or unequal axially symmetric deformed, oriented nuclei, lying in the same plane (azimuthal angle $\Phi = 0^\circ$) for various θ_1 and θ_2 values in the range 0° – 180° . The θ_i are measured anticlockwise from the colliding axis and angle α_i in clockwise from the symmetry axis.

θ_i , and the azimuthal angle Φ ($= 0^\circ$ for two nuclei lying in the same plane, as shown in Fig. 1). In terms of these coordinates, for ℓ partial waves, we define for each fragmentation (A_1, A_2), the CN decay or formation cross section

$$\sigma_{(A_1, A_2)} = \frac{\pi}{k^2} \sum_{\ell=0}^{\ell_{\text{max}}} (2\ell + 1) P_0 P; \quad k = \sqrt{\frac{2\mu E_{c.m.}}{\hbar^2}}, \quad (1)$$

where P_0 is the preformation probability referring to η motion at a fixed R value and P , the penetrability, to R motion for each η , both dependent on angular momentum ℓ and temperature T . μ is the reduced mass. ℓ_{max} is the maximum angular momentum, defined for light-particles evaporation residue cross section $\sigma_{\text{ER}} \rightarrow 0$.

The same formula as above is applicable to the noncompound, quasifission (qf) decay process, where $P_0 = 1$ for the incoming channel since for qf process the target and projectile nuclei can be considered to have not yet lost their identity. Then, for P calculated as for the incoming channel η_{ic} ,

$$\sigma_{\text{qf}} = \frac{\pi}{k^2} \sum_{\ell=0}^{\ell_{\text{max}}} (2\ell + 1) P_{\eta_{ic}}. \quad (2)$$

Thus, in DCM, the cross section for each (pair of) decay product is calculated as emission of preformed cluster(s) through their interaction barrier. Noting that Eq. (1) is defined in terms of the exit or decay channels alone, i.e., both the formation P_0 and then their emission via barrier penetration P are calculated only for decay channels (A_1, A_2), it follows from Eq. (1) that

$$\sigma_{\text{ER}} = \sum_{A_2=1}^{4 \text{ OR } 5} \sigma_{(A_1, A_2)} \quad \text{OR} \quad = \sum_{x=1}^{4 \text{ OR } 5} \sigma_{xn}, \quad (3)$$

and

$$\sigma_{\text{ff}} = 2 \sum_{A/2-x}^{A/2} \sigma_{(A_1, A_2)}, \quad (4)$$

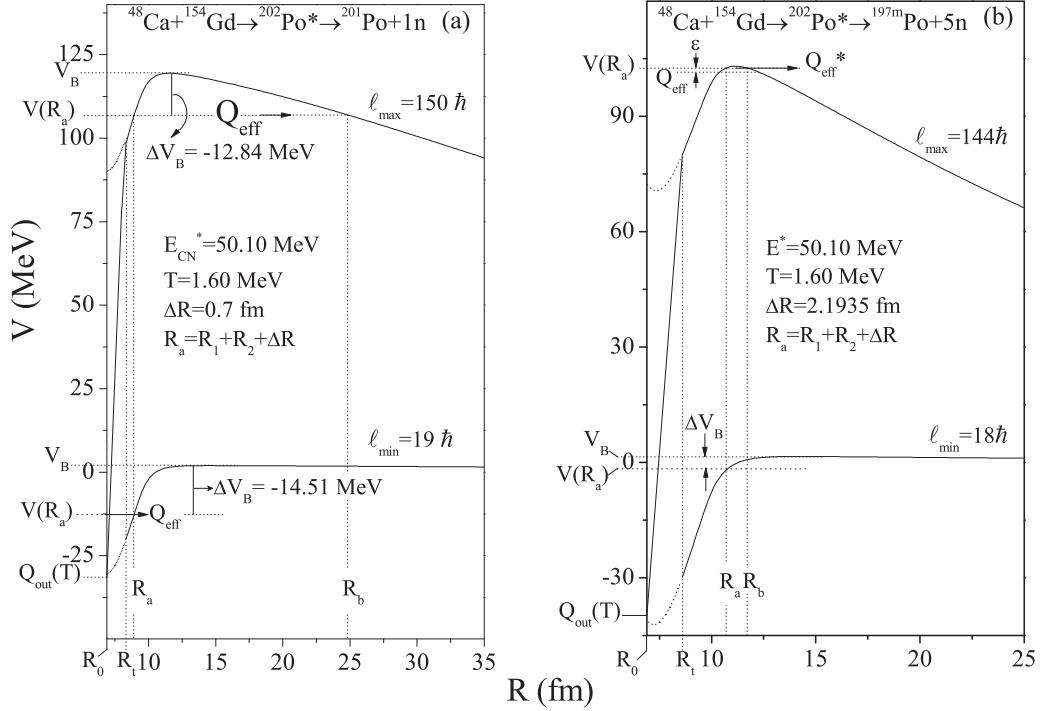


FIG. 2. The temperature (T) and ℓ -dependent scattering potential $V(R)$ in (a) the g.s. decay of $^{202}\text{Po}^*$ to $^{201}\text{Po} + 1n$, and (b) the decay of $^{202}\text{Po}^*$ to metastable ^{197m}Po state, i.e., $^{202}\text{Po}^* \rightarrow ^{197m}\text{Po} + 5n$ decay channel, both at $E_{\text{CN}}^* = 50.10$ MeV ($T = 1.60$ MeV). The first and second turning points R_a and R_b are labeled, and the barrier lowering parameter $\Delta V_B = V(R_a) - V_B$ is shown for both the $\ell_{\text{max}} = 150 \hbar$ and $\ell_{\text{min}} = 19 \hbar$ values. The scattering potential from touching radius R_t up to spherical CN radius R_0 is extrapolated as a polynomial. The decay path, defined by $V(R_a, \ell) = Q_{\text{eff}}$ for g.s. to g.s., and by $V(R_a, \ell) = Q_{\text{eff}}^*$ for g.s. to m.s. is shown to begin at $R_a (= R_t + \Delta R)$ for both cases.

giving $\sigma_{\text{CN}} = \sigma_{\text{ER}} + \sigma_{\text{ff}}$, and $\sigma_{\text{fusion}} = \sigma_{\text{CN}} + \sigma_{\text{qf}}$. Then, for each ℓ , the preformation yields $P_0(A_i)$ of fragments A_i are given by the solution of the stationary Schrödinger equation in η , at a fixed $R = R_a$,

$$\left\{ -\frac{\hbar^2}{2\sqrt{B_{\eta\eta}}} \frac{\partial}{\partial \eta} \frac{1}{\sqrt{B_{\eta\eta}}} \frac{\partial}{\partial \eta} + V(R, \eta, T) \right\} \psi^\nu(\eta) = E^\nu \psi^\nu(\eta), \quad (5)$$

with $\nu = 0, 1, 2, 3, \dots$ referring to ground-state ($\nu = 0$) and excited-state solutions. The mass parameters, $B_{\eta\eta}$, used are the smooth classical hydrodynamical masses [26], since at large T values the shell effects are almost completely washed out. For smaller T (< 1.5 MeV), in principle, the shell corrected masses, such as the cranking masses, which depend on the underlying shell-model basis, should be used. The preformation probability $P_0 = |\psi[\eta(A_i)]|^2 \sqrt{B_{\eta\eta} \frac{2}{A}}$.

The collective fragmentation potential $V_R(\eta, T)$ in Eq. (5), which brings in the structure effects of the CN in to the formalism, is calculated according to the Strutinsky renormalization procedure ($B = V_{\text{LDM}} + \delta U$; B is binding energy), as

$$V_R(\eta, T) = - \sum_{i=1}^2 [V_{\text{LDM}}(A_i, Z_i, T)] + \sum_{i=1}^2 [\delta U_i] \exp\left(-\frac{T^2}{T_0^2}\right) + V_P(R, A_i, \beta_{\lambda i}, \theta_i, T) + V_C(R, Z_i, \beta_{\lambda i}, \theta_i, T) + V_\ell(R, A_i, \beta_{\lambda i}, \theta_i, T), \quad (6)$$

where V_C , V_P , and V_ℓ are the temperature- and orientation-dependent Coulomb, nuclear proximity and angular-momentum-dependent potentials, respectively [16]. δU are the empirical shell corrections of Myers and Swiatecki [27] for spherical nuclei, also made T dependent to vanish exponentially with $T_0 = 1.5$ MeV [28], and V_{LDM} is T -dependent liquid drop energy of Davidson *et al.* [29] with its constants at $T = 0$ refitted by some of us [30–32] to give the experimental binding energies of Audi *et al.* [33] or that of Möller *et al.* [34] wherever not available in Ref. [33]. The fact that we are using experimental binding energies, split into V_{LDM} and δU components, means to bring into the calculations the deformation effects of nuclei, at least to some extent.

The scattering potential $V(R)$ for a fixed η value is illustrated in Fig. 2(a) for the g.s. to g.s. decay, and in Fig. 2(b) for g.s. to m.s. decay. For decays to metastable states of $3n$ and $5n$ fragments, i.e., to ^{199m}Po and ^{197m}Po , $V_R(\eta, T)$ in Eq. (6) is modified, each, by the difference in energy of g.s. with respect to (w.r.t.) m.s., denoted $\varepsilon_j, j = xn, x = 3, 5$ [see Figs. 3(b), 3(c), and Eq. (9) below for the \pm sign of ε_j]. The penetrability P in Eq. (1) or Eq. (2) is the WKB integral,

$$P = \exp\left(-\frac{2}{\hbar} \int_{R_a}^{R_b} \{2\mu[V(R, T) - Q_{\text{eff}}]\}^{1/2} dR\right), \quad (7)$$

solved analytically [35,36], with the second turning point R_b [see Fig. 2(a)] satisfying

$$V(R_a) = V(R_b) = Q_{\text{eff}}, \quad (8)$$

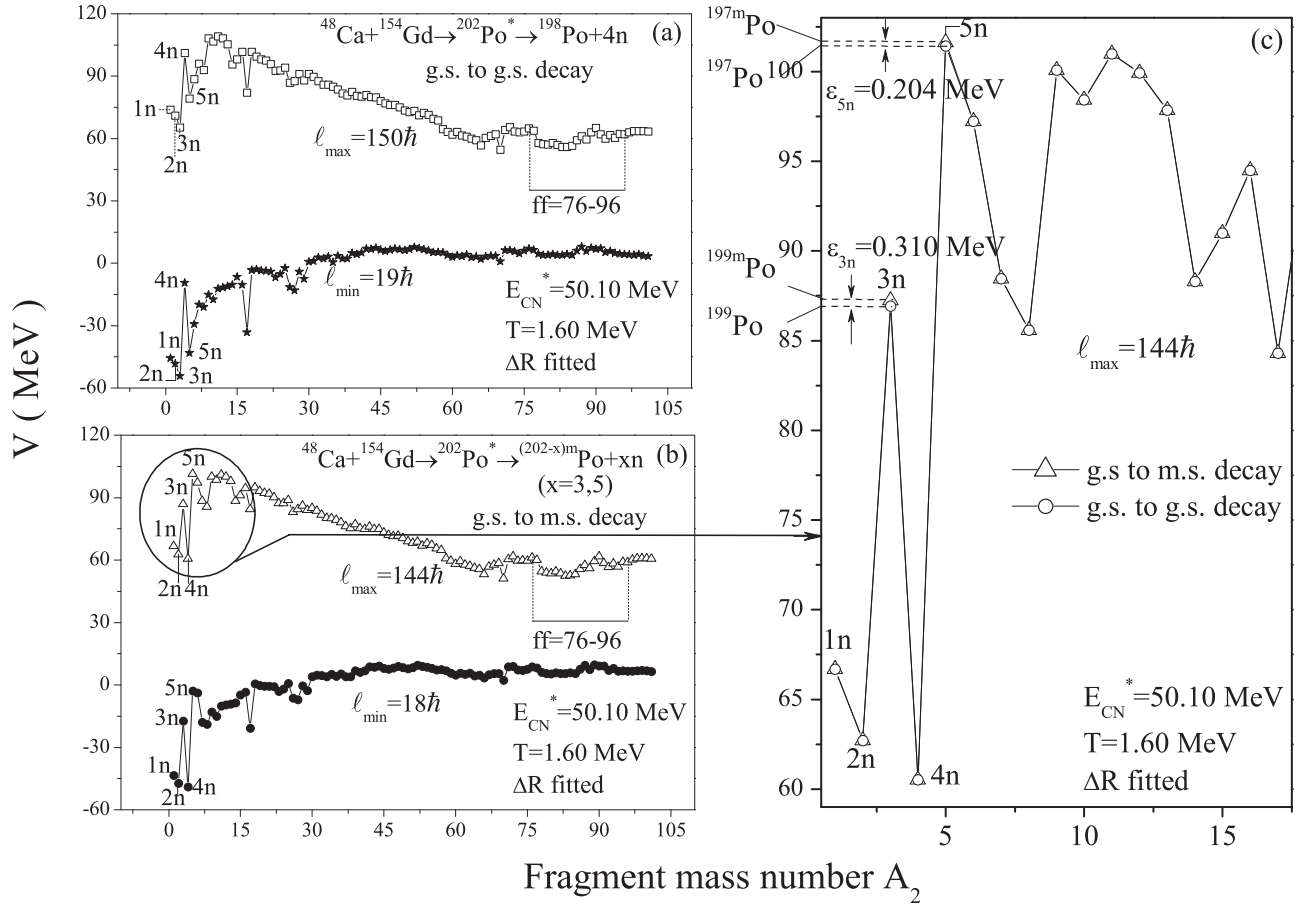


FIG. 3. Fragmentation potentials $V(A_2)$, as a function of light fragment mass number A_2 , for (a) the g.s. decay of $^{202}\text{Po}^*$ formed in $^{48}\text{Ca} + ^{154}\text{Gd}$ reaction, plotted at ℓ_{\min} and ℓ_{\max} values, for best-fitted ΔR values given in Table I Cal.2 for xn decay channels, at $E_{\text{CN}}^* = 50.10$ MeV, using quadrupole deformations (β_{2i}) alone with θ_i^{opt} orientations. The fusion-fission (ff) region is also marked; (b) decay of $^{202}\text{Po}^*$ to metastable states, plotted at ℓ_{\min} and ℓ_{\max} values, for best-fitted ΔR values given in Table II Cal.2. Figure 3(c) shows a magnified view of the fragmentation potential, modified due to $3n$ and $5n$ metastable states ^{199m}Po and ^{197m}Po , i.e., how the respective metastable state energy difference (ε_j) is added to their respective g.s., i.e., fragmentation potential $V^m(xn) = V(xn) + \varepsilon_j$, $j = xn$ (and their complementary heavy fragments), where $\varepsilon_j = 0.31$ MeV for $j = 3n$ and 0.204 MeV for $j = 5n$ [12].

Q_{eff} being the effective Q value for the g.s. to g.s. decay. For g.s. to m.s. decay of the same nucleus, the Q value gets modified to a Q value given by the Q value for the g.s. to g.s. decay minus or plus the excitation energy ε , i.e., the metastable-state energy difference w.r.t. its ground state. The Q_{eff} value in Eq. (7) is then replaced by [37],

$$Q_{\text{eff}}^* = Q_{\text{eff}} \pm \varepsilon, \quad (9)$$

(+) or (−) depending on the metastable (excited) state lying above or below the ground state. This is illustrated in Fig. 2(b).

For the decay of hot CN, the first turning point R_a , defining the point of fragment or cluster preformation P_0 , and the penetration path for calculating penetrability P , is postulated by Gupta *et al.* [30,31] as,

$$\begin{aligned} R_a(T) &= R_1(\alpha_1, T) + R_2(\alpha_2, T) + \Delta R(\eta, T), \\ &= R_i(\alpha, \eta, T) + \Delta R(\eta, T), \end{aligned} \quad (10)$$

Thus, the only parameter of the model is the T -dependent $\Delta R(T)$, the neck-length [or barrier-lowering ΔV_B , refer to Eq. (13)] parameter, which assimilates the deformation and

neck formation effects between two nuclei, introduced within the extended orbiting cluster model of Gupta and collaborators [38–40]. This method of introducing a neck-length parameter ΔR is similar to that used in both the scission-point [41] and saddle-point [42–44] statistical fission models. The R_i in Eq. (10) are the radius vectors given by

$$R_i(\alpha_i, T) = R_{0i}(T) \left[1 + \sum_{\lambda} \beta_{\lambda i} Y_{\lambda}^{(0)}(\alpha_i) \right] \quad (11)$$

and T -dependent radii $R_{0i}(T)$ for the equivalent spherical nuclei [45],

$$R_{0i} = [1.28A_i^{1/3} - 0.76 + 0.8A_i^{-1/3}](1 + 0.0007T^2). \quad (12)$$

The angles α_i of radius vectors are measured in the clockwise direction from the nuclear symmetry axis and the orientation angles θ_i are measured anticlockwise from the collision Z axis (see Fig. 1).

Next, the potential at first turning point $V(R_a, \ell)$ is related to the top of the barrier $V_B(\ell)$ for each ℓ value, by defining

their difference $\Delta V_B(\ell)$ as the effective lowering of the barrier

$$\Delta V_B(\ell) = V(R_a, \ell) - V_B(\ell). \quad (13)$$

Note, ΔV_B for each ℓ is defined as a negative quantity since the actually used barrier is effectively lowered. The $\Delta R(T)$, the barrier lowering parameter, is generally positive but it can take negative values as well. The negative $\Delta R(T)$ value occurs as R_a (the first turning point of the penetration path) can always be chosen to start from $R_0(T)$ (radius for the equivalent spherical compound nucleus). Thus, the fitting parameter ΔR controls the barrier lowering and can take values such that $R_0 \leq R_a \leq R_B$, the interaction barrier R_B . This is illustrated in Fig. 2.

The compound nucleus temperature T (in MeV) is given by

$$E_{\text{CN}}^* = E_{c.m.} + Q_{\text{in}} = (A/10)T^2 - T, \quad (14)$$

with Q_{in} as the entrance or incoming channel Q value. Furthermore, the compound nucleus fusion/formation probability P_{CN} [46] is defined as

$$P_{\text{CN}} = \frac{\sigma_{\text{CN}}}{\sigma_{\text{fusion}}} = 1 - \frac{\sigma_{\text{qf}}}{\sigma_{\text{fusion}}}, \quad (15)$$

and the compound nucleus survival probability P_{surv} [47], the probability that the fused system will deexcite by emission of neutrons or LPs (equivalently, the ER) rather than fission, as

$$P_{\text{surv}} = \frac{\sigma_{\text{ER}}}{\sigma_{\text{CN}}} = 1 - \frac{\sigma_{\text{ff}}}{\sigma_{\text{CN}}}, \quad (16)$$

where the (total) fusion cross section $\sigma_{\text{fusion}} = \sigma_{\text{CN}} + \sigma_{\text{qf}}$ with σ_{CN} as the CN formation cross section (sum of ER and ff cross sections, $\sigma_{\text{CN}} = \sigma_{\text{ER}} + \sigma_{\text{ff}}$), and σ_{qf} as the noncompound (nCN), quasifission cross section.

III. CALCULATIONS AND RESULTS

In this section, we first study the decay of ²⁰²Po* CN to the ground state of ¹⁹⁸Po by emission of $4n$. Next, in Sec. III B, the decay mechanism of ²⁰²Po* to metastable states ^{199m}Po and ^{197m}Po is discussed. As already stated in Sec. I, our calculations are made for hot-compact configurations, supporting asymmetric fission of ²⁰²Po*.

A. Decay of ²⁰²Po* CN in ground state to the ground state of ¹⁹⁸Po

DCM has only one parameter, the neck-length parameter ΔR ($\equiv R_a$), to be used to fit the measured xn -decay channel cross sections σ_{xn} , whose sum gives the (total) evaporation residue cross section $\sigma_{\text{ER}} (= \sum \sigma_{xn}$, where $x = 1-5$; in the present case $x = 4$ only). Thus, two cases arise: (i) a single, fixed ΔR for each measured σ_{ER} at a given E_{CN}^* , i.e., the same ΔR (equivalently, same reaction time) for all xn -decay channels, without caring about the fitting of the individual channel cross sections; (ii) different ΔR 's for different decay channels, i.e., different reaction times for different decay channels, best fitting simultaneously all individual channel cross sections. Each of these two calculations, referred to as Cal.1 and Cal.2, are made at five E_{CN}^* 's ($= 41.03, 43.16, 45.22, 50.10, \text{ and } 53.61$ MeV), and compared with experimental data in Table I, discussed separately in the following two subsections. The important point to note is that Cal.1 gives only

the summed $\sigma_{\text{ER}} (= \sum \sigma_{xn})$, but not the measured individual decay channel cross sections σ_{xn} .

1. A single, fixed neck-length parameter ΔR to fit σ_{ER} in decay of CN ²⁰²Po*

For the decay of ²⁰²Po* CN to g.s. of ¹⁹⁸Po, in the fragmentation potential $V(A_2)$ [illustrated in Fig. 3(a) for case (ii)], first the minimized fragments for the masses $A_2 = 1-5$ are replaced by the binding energies of the respective neutron-decay channels $1n-5n$. A fixed value of ΔR is used to best fit the summed-up, measured ER cross section $\sigma_{\text{ER}} (= \sum \sigma_{xn}$, where $x = 4$), at each E_{CN}^* . The calculated σ_{ER} are presented as Cal.1 in Table I for all the five excitation energies. We notice in Table I (Cal.1) that the unobserved ($1n-3n, 5n$) cross sections are strongly overestimated, in particular for $1n$ and $2n$, and the observed $4n$ decay channel cross section σ_{4n} is strongly underestimated. In other words, in complete disagreement with experiments, the total strength of σ_{ER} is carried away by $1n$ -decay fragment alone. Apparently, Cal.1 in Table I is a very poor presentation of the model calculations, and hence we do not pursue it any further, rather go over in the following to case (ii), denoted as Cal.2, of simultaneously fitting of all individual channel cross sections.

2. Best-fitted ΔR 's for simultaneous fit of all decay channel cross sections σ_{xn}

Table I, Cal.2 shows our calculations of taking different ΔR value for each decay channel, i.e., different reaction time scales for different decay channels, making the unobserved $1n, 2n, 3n$, and $5n$ cross sections as small as possible (compared to zero). Then, the observed $4n$ decay channel requires noncompound nucleus (nCN) contribution, treated here as the quasifissionlike process: estimated empirically as $\sigma_{\text{qf}}^{\text{emp}} = \sigma_{xn}^{\text{Expt.}} - \sigma_{xn}^{\text{Cal.}}$, and fitted independently with preformation probability $P_0 = 1$. The relevant fragmentation potential $V(A_2)$, calculated for the decay of CN ²⁰²Po*, formed via ⁴⁸Ca + ¹⁵⁴Gd reaction at $T = 1.60$ MeV, corresponding to excitation energy $E_{\text{CN}}^* = 50.10$ MeV, for $\ell_{\text{max}} = 150 \hbar$ and $\ell_{\text{min}} = 19 \hbar$, using the best fitted ΔR 's (see Table I Cal. 2), is presented in Fig. 3(a). The minimized fragments for masses $A_2 = 4$ and 5 were ⁴H and ⁵He, which were replaced by the binding energies of the fragments of interest, i.e., the observed neutron-decay channels $4n$ and $5n$. The fusion-fission (ff) region, for similar depths of minima in $V(A_2)$, is also marked in Fig. 3(a) as $A_2 = 76-96$. The ℓ_{max} and ℓ_{min} values are fixed, respectively, for the calculated P_0 and P as functions of ℓ , presented in Figs. 4(a) and 5(a) for $xn, x = 1-5$ decay channels. Fig. 4(a) shows that $3n$ has maximum preformation probability followed by $2n, 1n, 5n$, and $4n$ and for $P_0 > 10^{-11}$, we can fix the limiting value $\ell_{\text{max}} = 150 \hbar$, although it is slightly different for different decay channels, but then not contributing. Similarly, in Fig. 5(a), the contribution of P goes on increasing as the ℓ value increases, setting the limiting $\ell_{\text{min}} = 19 \hbar$ where $P > 10^{-30}$, although it is much larger for $1n-3n$ and $5n$ but again would not contribute. Furthermore, the P in Fig. 5(a) illustrates that it is maximum for observed $4n$ decay channel followed by $1n, 2n, 3n$, and $5n$. P_0 for $3n, 2n$, and $1n$ are maximum whereas their penetrability P in Fig. 5(a) are lowest. The combined

TABLE I. DCM calculated evaporation residue cross section $\sigma_{ER} = \sum_{x=1}^5 \sigma_{xn}$ with Cal.1 as a best-fitted single fixed ΔR and Cal.2 as individually fitted channel cross section σ_{xn} for g.s. decay of $^{202}\text{Po}^*$, formed in $^{48}\text{Ca} + ^{154}\text{Gd}$ reaction, to ground state of ^{198}Po at various E_{CN}^* 's, giving the CN contribution σ_{xn}^{CN} , the empirical nCN quasifission (qf) cross section $\sigma_{qf}^{emp} = \sigma_{xn}^{Expt.} - \sigma_{xn}^{CN}$, and their sum, the calculated channel cross section $\sigma_{xn}^{Cal.} = \sigma_{xn}^{CN} + \sigma_{qf}^{Cal.}$, compared with experimental data. The predicted ff cross sections $\sigma_{ff}^{pred.}$ for the best fitted ΔR -values, are also given.

Decay-channel	Cal.1 (Fixed ΔR)		Cal.2 (Channel cross section Fitted ΔR)						
	$\sigma_{xn}^{Cal.}$	$\sigma_{xn}^{Expt.}$	CN contribution		qf contribution		$\sigma_{xn}^{Cal.} =$	$\sigma_{ff}^{pred.}$ (mb)	
	(mb)	(mb)	ΔR	σ_{xn}^{CN}	σ_{qf}^{emp}	ΔR	$\sigma_{qf}^{Cal.}$	$\sigma_{xn}^{CN} + \sigma_{qf}^{Cal.}$	
$E_{CN}^* = 41.03 \text{ MeV } T = 1.45 \text{ MeV}$									
$\Delta R = 1.3435 \text{ fm}$									
1n	0.696	—	0.7	3.92×10^{-7}	—	—	—	3.92×10^{-7}	
2n	3.77×10^{-3}	—	0.0	5.88×10^{-13}	—	—	—	5.88×10^{-13}	
3n	1.88×10^{-5}	—	-1.5	3.85×10^{-21}	—	—	—	3.85×10^{-21}	
4n	3.76×10^{-8}	0.7 ± 0.1	2.342	0.7	0.0	—	—	0.7	
5n	5.57×10^{-11}	—	-1.4	3.12×10^{-29}	—	—	—	3.12×10^{-29}	
σ_{ER}	0.7	0.7		0.7	0.0			0.7	424.0
$E_{CN}^* = 43.16 \text{ MeV } T = 1.49 \text{ MeV}$									
$\Delta R = 1.4206 \text{ fm}$									
1n	2.09	—	0.7	3.92×10^{-7}	—	0.1	4.68×10^{-8}	4.39×10^{-7}	
2n	1.28×10^{-2}	—	0.0	5.32×10^{-13}	—	0.1	8.84×10^{-9}	8.84×10^{-9}	
3n	8.55×10^{-5}	—	-1.5	3.59×10^{-21}	—	0.1	1.62×10^{-9}	1.62×10^{-9}	
4n	1.97×10^{-7}	2.1 ± 0.3	2.608	1.12	0.98	1.1573	0.98	2.10	
5n	3.02×10^{-10}	—	-1.4	2.65×10^{-29}	—	0.1	5.82×10^{-10}	5.82×10^{-10}	
σ_{ER}	2.10	2.10		1.12	0.98		0.98	2.10	324.0
$E_{CN}^* = 45.22 \text{ MeV } T = 1.52 \text{ MeV}$									
$\Delta R = 1.4331 \text{ fm}$									
1n	2.49	—	0.7	3.97×10^{-7}	—	0.1	4.45×10^{-8}	4.42×10^{-7}	
2n	1.68×10^{-2}	—	0.0	5.24×10^{-13}	—	0.1	8.37×10^{-9}	8.37×10^{-9}	
3n	1.30×10^{-4}	—	-1.5	3.83×10^{-21}	—	0.1	1.55×10^{-9}	1.55×10^{-9}	
4n	3.36×10^{-7}	2.5 ± 0.4	2.612	1.11	1.39	1.1812	1.39	2.50	
5n	5.69×10^{-10}	—	-1.4	2.83×10^{-29}	—	0.1	5.47×10^{-10}	5.47×10^{-10}	
σ_{ER}	2.50	2.50		1.11	1.39		1.39	2.50	230.0
$E_{CN}^* = 50.10 \text{ MeV } T = 1.60 \text{ MeV}$									
$\Delta R = 1.4695 \text{ fm}$									
1n	3.97	—	0.7	3.61×10^{-7}	—	0.1	3.96×10^{-8}	4.01×10^{-7}	
2n	3.5×10^{-2}	—	0.0	4.38×10^{-13}	—	0.1	7.39×10^{-9}	7.39×10^{-9}	
3n	3.65×10^{-4}	—	-1.5	3.25×10^{-21}	—	0.1	1.32×10^{-9}	1.32×10^{-9}	
4n	1.19×10^{-6}	4.0 ± 0.6	2.62	1.05	2.95	1.235	2.95	4.0	
5n	2.36×10^{-9}	—	-1.4	2.53×10^{-29}	—	0.1	4.74×10^{-10}	4.74×10^{-10}	
σ_{ER}	4.0	4.0		1.05	2.95		2.95	4.0	73.8
$E_{CN}^* = 53.61 \text{ MeV } T = 1.65 \text{ MeV}$									
$\Delta R = 1.4452 \text{ fm}$									
1n	2.87	—	0.7	3.26×10^{-7}	—	0.1	3.59×10^{-8}	3.62×10^{-7}	
2n	2.86×10^{-2}	—	0.0	4.40×10^{-13}	—	0.1	6.77×10^{-9}	6.77×10^{-9}	
3n	3.55×10^{-4}	—	-1.5	3.61×10^{-21}	—	0.1	1.21×10^{-9}	1.21×10^{-9}	
4n	1.25×10^{-6}	2.9 ± 0.5	2.62	1.03	1.87	1.2106	1.87	2.9	
5n	2.65×10^{-9}	—	-1.4	2.99×10^{-29}	—	0.1	4.29×10^{-10}	4.29×10^{-10}	
σ_{ER}	2.9	2.9		1.03	1.87		1.87	2.9	45.0

effect of P_0 and P , i.e., the variation of channel cross section σ_{xn} as a function of ℓ in Fig. 6(a) shows that the ℓ 's contributing to σ_{xn} has the limiting values $\ell_{min} < \ell < \ell_{max}$, and that for the best-fitted ΔR 's used here, the decay cross sections for unobserved 1n, 2n, 3n, and 5n channels are negligible while it

is maximum for 4n decay channel, the experimentally observed channel.

Following the above procedure, the DCM calculated pure CN channel cross section σ_{xn}^{CN} and the nCN, qf cross section are obtained, whose sum gives $\sigma_{xn}^{Cal.}$, compared with $\sigma_{xn}^{Expt.}$

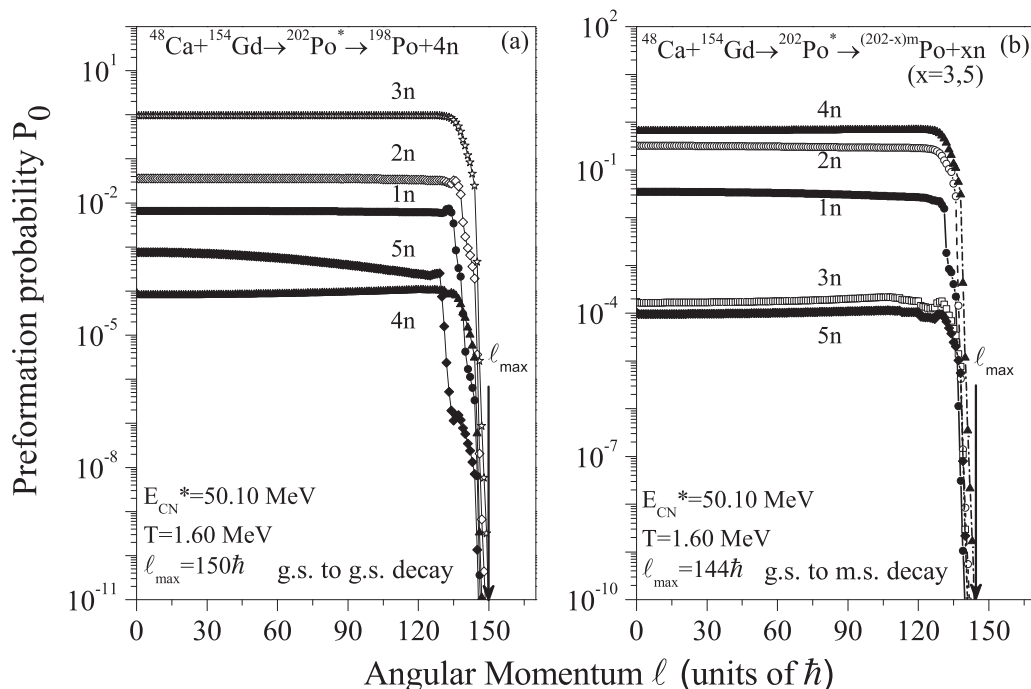


FIG. 4. The preformation probability P_0 vs. angular momentum l for the fragmentation potential (a) for g.s. to g.s. decay of $^{202}\text{Po}^*$, and (b) for g.s. to m.s. decays of $^{202}\text{Po}^*$.

for all the five E_{lab} , or E_{CN}^* in Table I Cal.2. Note that for g.s. to g.s. decay, only $x = 4$ channel is observed. Also, the fusion-fission (ff) cross section are estimated, shown in Table I as the predicted ff cross sections $\sigma_{\text{ff}}^{\text{pred}}$. Thus, Table I Cal.2 shows that our DCM calculated xn channel cross sections compare nicely with the measured channel cross sections $\sigma_{xn}^{\text{Expt}}$.

only when significant noncompound qf content is allowed. This is illustrated in Fig. 7(a) where the CN contribution $\sigma_{\text{ER}}^{\text{CN}}$ as well as the nCN, qf content $\sigma_{\text{qf}}^{\text{Cal}}$, together with their sum σ_{xn}^{Cal} is compared with experimental data [8] on $\sigma_{xn}^{\text{Expt}}$ and the other available statistical model calculation [8]. Our DCM calculations are apparently better, but with a considerable

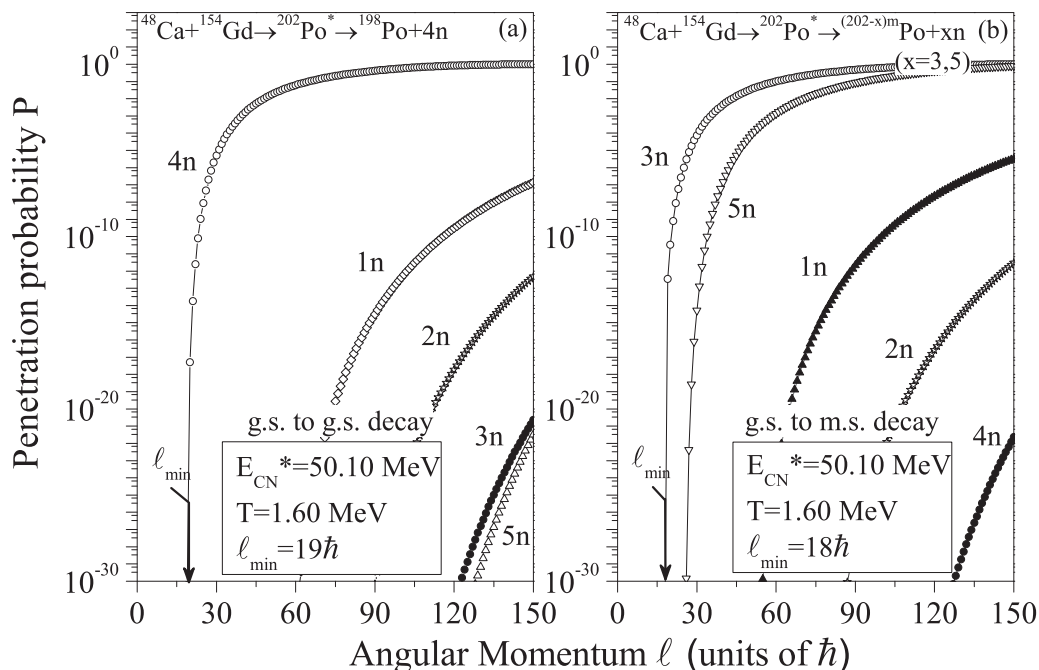


FIG. 5. Same as for Fig. 4, but for penetrability P .

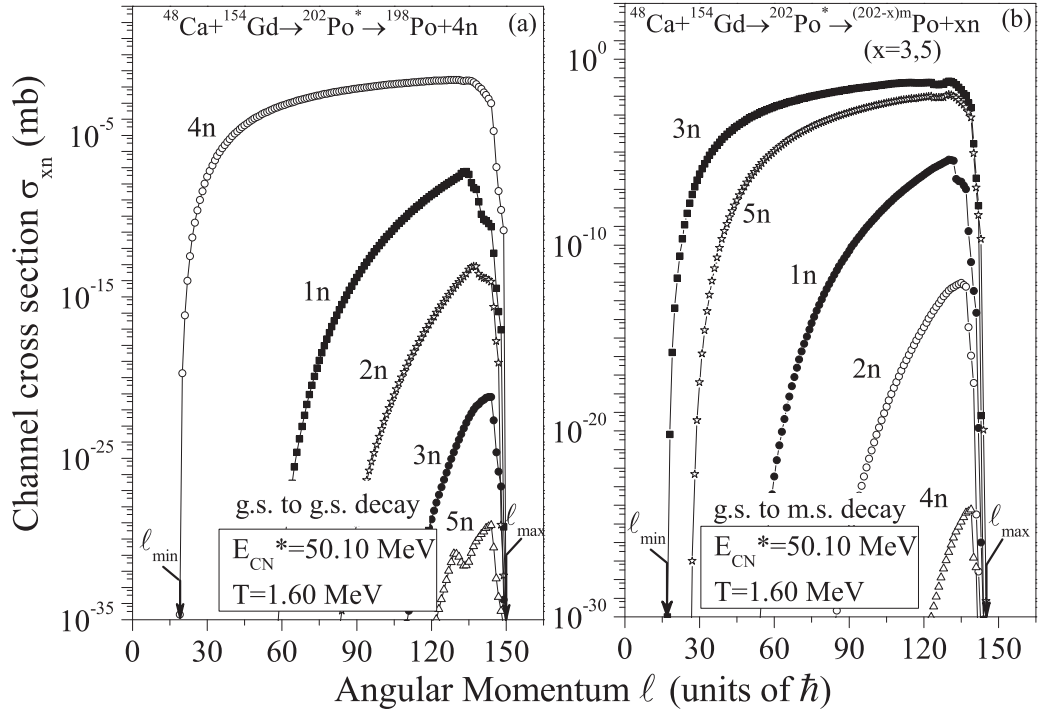


FIG. 6. The xn decay channel cross sections σ_{xn} , $x = 1-5$, vs. angular momentum ℓ as per details in Fig. 4 for (a) g.s. to g.s. decay, and (b) g.s. to m.s. decays.

amount of nCN contribution $\sigma_{qn}^{Cal.}$ (refer to dotted line with open, down-triangles), varying from zero to a maximum of

$\sim 70\%$ of the total channel cross section $\sigma_{xn}^{Cal.}$ ($= \sigma_{xn}^{CN} + \sigma_{qn}^{Cal.}$; refer to open squares with solid line).

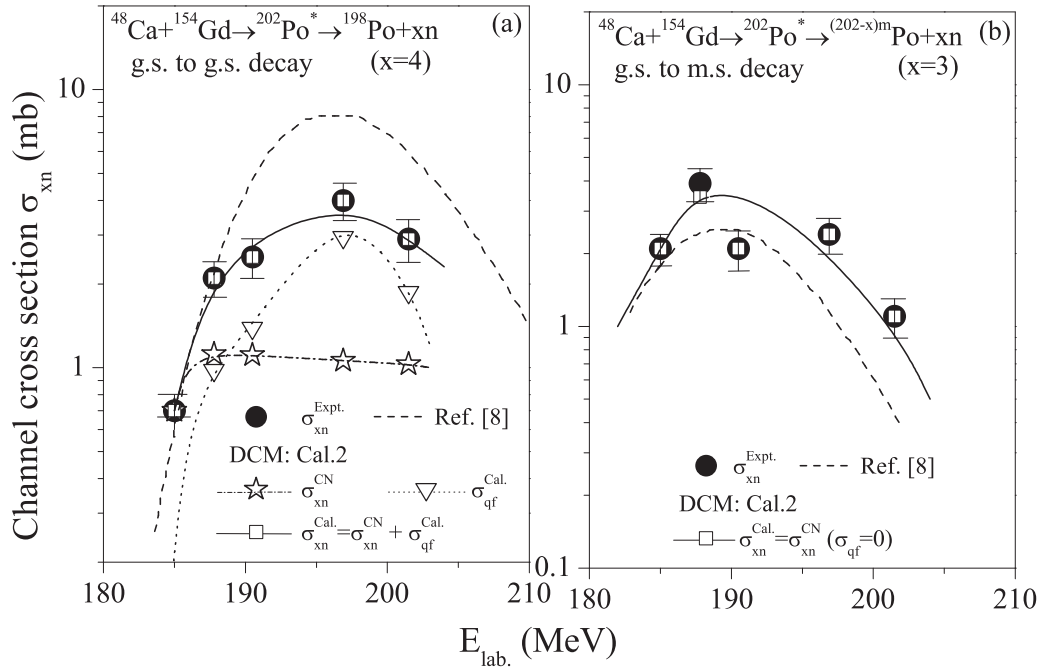


FIG. 7. (a) DCM calculated σ_{xn} excitation functions for g.s. decay of $^{202}\text{Po}^*$ for best fitted ΔR 's in Table I Cal.2, composed of the pure CN contribution σ_{xn}^{CN} (dash-dot line with open stars) and the noncompound quasifission component $\sigma_{qn}^{Cal.}$ (dotted line with open down-triangles), and their sum $\sigma_{xn}^{Cal.}$ (solid line with open squares; lines are a guide for the eyes), compared with experimental data (filled circles), and a statistical model calculation (dashed line [8]). (b) DCM calculated σ_{xn} excitation functions of $^{202}\text{Po}^*$ for decay to metastable state $x = 3$ for best-fitted ΔR 's in Table II Cal.2 (open squares, with solid lines as a guide for the eyes), compared with experimental data (filled circles) and the above-stated statistical model calculation (dashed line [8]).

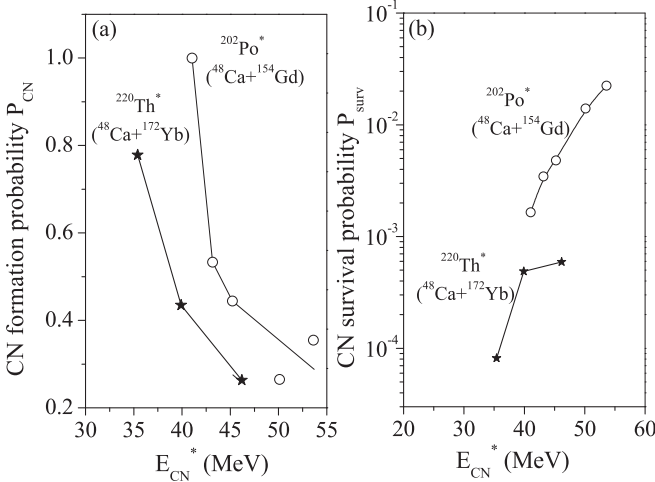


FIG. 8. Variation of DCM calculated (a) P_{CN} and (b) P_{surv} as a function of excitation energy E_{CN}^* for the g.s. decay of $^{202}\text{Po}^*$, for β_{2i} -deformed $\theta_i^{opt.}$, and $\Phi = 0^\circ$ case, compared with another ^{48}Ca -induced reaction [10] forming $^{220}\text{Th}^*$.

Next, Fig. 8 shows the variation of DCM calculated CN formation probability P_{CN} and the CN survival probability P_{surv} as a function of CN excitation energy E_{CN}^* for g.s. to g.s. decay of $^{202}\text{Po}^*$, compared with other available calculations for ^{48}Ca -induced reactions [6,7,10]. Note that our calculations (Ref. [10] and present ones) are for β_{2i} -deformed, $\theta_i^{opt.}$ and $\Phi = 0^\circ$ case. The interesting result of Fig. 8(a) is that $^{202}\text{Po}^*$ shows the same behavior as observed for $^{220}\text{Th}^*$, i.e., P_{CN} decreasing with increasing E_{CN}^* , also satisfying the range of P_{CN} obtained [8] for other ^{48}Ca -induced reactions [6,7] and the other radioactive CN [46]. Furthermore, this is also true of reactions, other than ^{48}Ca induced, forming the radioactive $^{220}\text{Th}^*$ [10]. Similarly, P_{surv} increases with increase of E_{CN}^* for the two ^{48}Ca -induced reactions in Fig. 8(b), as expected of radioactive CN in the DCM [47].

B. Decay of $^{202}\text{Po}^*$ in ground state to metastable states ^{199m}Po and ^{197m}Po

As already mentioned in the Introduction, CN $^{202}\text{Po}^*$ decays to metastable state ^{199m}Po alone for the first three excitation energies $E_{CN}^* = 41.03, 43.16,$ and 45.22 MeV, and to ^{199m}Po and ^{197m}Po (respectively, by $3n$ and $5n$ emissions), for the next two higher $E_{CN}^* = 50.10$ and 53.61 MeV, with metastable excitation energies $\varepsilon = 0.310$ and 0.204 MeV [12], above their respective ground states. For the DCM calculations, we consider the case (ii) of neck-length parameter ΔR fitted channel cross section σ_{xn} individually, i.e., of different reaction times for different decay channels, and hence use the fragmentation potential plotted in Fig. 3(b), where, in addition to replacing the binding energies of $A_2 = 1-5$ with that of $1n-5n$, the potential is modified by adding the metastable excitation energies $\varepsilon = 0.310$ and 0.204 MeV, respectively at $3n$ and $5n$ fragmentations, as is illustrated in Fig. 3(c), showing a magnified view of region concerned. This is referred to as Cal.2 in Table II, where we choose ΔR 's such that the channel cross sections σ_{xn} for the unobserved channels $x = 1,2,4,5$

TABLE II. DCM calculated individual channel cross sections σ_{xn} , denoted Cal. 2, for the decay of CN $^{202}\text{Po}^*$ to metastable ^{199m}Po and ^{197m}Po at various E_{CN}^* 's, compared with experimental data. Here, the nCN contribution, equivalently, the quasifission content, is zero. The predicted ff cross sections $\sigma_{ff}^{pred.}$ for the best-fitted ΔR values, are also given, which are nearly the same as for g.s. to g.s. decay.

Cal.2 (Channel cross section Fitted ΔR)				
Decay-channel	$\sigma_{xn}^{Expt.}$ (mb)	ΔR (fm)	$\sigma_{xn}^{Cal.}$ (mb)	$\sigma_{ff}^{pred.}$ (mb)
$E_{CN}^* = 41.03$ MeV $T = 1.45$ MeV				
$1n$	—	0.9	3.63×10^{-5}	
$2n$	—	0.1	6.40×10^{-12}	
$3n$	2.10 ± 0.3	2.508	2.10	
$4n$	—	-1.5	1.415×10^{-24}	
$5n$	—	1.2	3.3×10^{-5}	
σ_{ER}	2.10		2.10	428
$E_{CN}^* = 43.16$ MeV $T = 1.49$ MeV				
$1n$	—	1.3	3.01×10^{-3}	
$2n$	—	0.1	7.81×10^{-12}	
$3n$	3.9 ± 0.6	2.807	3.43	
$4n$	—	-1.6	2.82×10^{-24}	
$5n$	—	-0.8	8.26×10^{-25}	
σ_{ER}	3.9		3.43	328
$E_{CN}^* = 45.22$ MeV $T = 1.52$ MeV				
$1n$	—	0.9	3.33×10^{-5}	
$2n$	—	0.1	5.38×10^{-12}	
$3n$	2.10 ± 0.4	2.533	2.10	
$4n$	—	-1.5	1.55×10^{-24}	
$5n$	—	1.2	3.21×10^{-5}	
σ_{ER}	2.10		2.10	228
$E_{CN}^* = 50.10$ MeV $T = 1.60$ MeV				
$1n$	—	0.9	2.66×10^{-5}	
$2n$	—	0.1	4.41×10^{-12}	
$3n$	2.4 ± 0.4	2.7135	2.4	
$4n$	—	-1.5	9.76×10^{-25}	
$5n$	0.3 ± 0.1	2.1935	0.3	
σ_{ER}	2.70		2.70	76.6
$E_{CN}^* = 53.61$ MeV $T = 1.65$ MeV				
$1n$	—	1.3	1.96×10^{-3}	
$2n$	—	0.8	4.26×10^{-8}	
$3n$	1.1 ± 0.2	2.4295	1.10	
$4n$	—	-1.6	1.35×10^{-24}	
$5n$	1.0 ± 0.2	2.551	0.858	
σ_{ER}	2.10		2.10	48.6

are small for the first three lowest E_{CN}^* 's since σ_{3n} alone is observed, and for unobserved $x = 1,2,4$ it is small at the highest two energies where σ_{3n} and σ_{5n} are observed. Thus, the fragmentation potential $V(A_2)$ in Fig. 3(b) is illustrated for the decay of CN $^{202}\text{Po}^*$ to metastable states ^{199m}Po and ^{197m}Po (equivalently, $3n$ and $5n$) formed via $^{48}\text{Ca} + ^{154}\text{Gd}$ reaction at $T = 1.60$ MeV, corresponding to excitation energy $E_{CN}^* = 50.10$ MeV for $\ell_{max} = 144 \hbar$ and $\ell_{min} = 18 \hbar$, using the best-fitted ΔR 's in Table II Cal.2. The fusion-fission (ff) region is also marked, which remains the same both in range ($A_2 = 76-96$) as well as in magnitude of $\sigma_{ff}^{pred.}$ as for g.s.

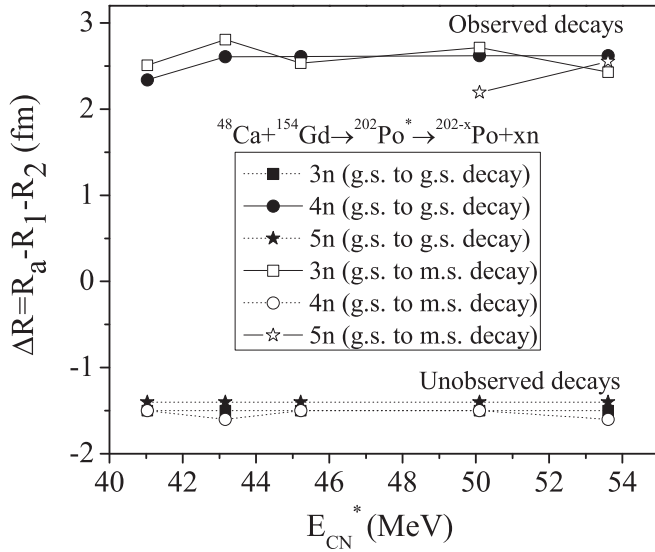


FIG. 9. Variation of DCM calculated ΔR with E_{CN}^* for the observed and unobserved g.s. to g.s. and g.s. to m.s. decays of $^{202}\text{Po}^*$.

to g.s. decay. The ℓ_{\max} and ℓ_{\min} values are obtained as per Figs. 4(b) and 5(b) or 6(b). Apparently, as the combined effect of P_0 and P , the observed decays to metastable states $3n$ and $5n$ channels are now more predominant [see the channel cross section in Fig. 6(b)], compared to $4n$ decay in g.s. to g.s. decay [see Fig. 6(a)].

Using the above-stated fragmentation potential $V(A_2)$ in Fig. 3(b) and the corresponding scattering potential $V(R)$ in Fig. 2(b) where Q_{eff}^* replaces Q_{eff} , respectively, for $3n$ (and $5n$) decays (see Sec. II), we observe in Table II that the metastable $3n$ and $5n$ states are fitted exactly (within experimental error bars, at some incident energies) without any qf-like noncompound nucleus contribution, i.e., $\sigma_{\text{qf}} = 0$. Thus, the decay of CN $^{202}\text{Po}^*$ to metastable ^{199m}Po , ^{197m}Po states are shown to be the pure CN decays. This is further illustrated in Fig. 7(b) for σ_{3n} decay channel, compared with another model calculation [8]. Apparently, our fits to data are clearly better, proving thereby that the observed g.s. to m.s. ^{199m}Po and ^{197m}Po decays (respectively, the $3n$ and $5n$ emissions) are the pure CN decays, compared to $4n$ or ^{198}Po g.s. to g.s. decay where a substantial amount of nCN, quasifission decay cross section is required. Also, in Table II are shown the fusion-fission (ff) cross sections $\sigma_{\text{ff}}^{\text{pred.}}$ for the g.s. to m.s. decays, which compare nearly exactly with g.s. to g.s. decays.

Finally, Fig. 9 shows the variation of best-fitted ΔR vs. E_{CN}^* for both the g.s. to g.s. and g.s. to m.s. (refer to Tables I and II, respectively) decays of $^{202}\text{Po}^*$ via $3n, 4n$, and $5n$ emission. Interestingly, the observed ($4n$ in g.s. to g.s. and

$3n$ and $5n$ in g.s. to m.s. decays, respectively) and unobserved decays are clustered around two nearly constant ΔR values: $\Delta R_{\text{observed}} = 2.45 \pm 0.20$ and $\Delta R_{\text{unobserved}} = -1.48 \pm 0.05$ fm; the observed decays occurring first since $\Delta R_{\text{observed}} \gg \Delta R_{\text{unobserved}}$. This result gives an unspoken strength to our model, and hence is useful for making predictions.

IV. SUMMARY AND CONCLUSIONS

In this paper, the decay of CN $^{202}\text{Po}^*$ to g.s. of ^{198}Po and to metastable states ^{199m}Po and ^{197m}Po are studied within the framework of the QMFT-based DCM, which has a single parameter ΔR , neck-length, or barrier-lowering parameter ΔV_B . We have analyzed both the g.s. to g.s. and g.s. to m.s. decays of $^{202}\text{Po}^*$ separately. All calculations, for both types of decays, are made for quadrupole deformations β_{2i} and optimum orientations $\theta_i^{\text{opt.}}$ of coplanar ($\Phi = 0^\circ$) nuclei, using hot fusion configurations since it supports the asymmetric fission mass distribution of $^{202}\text{Po}^*$, observed in neighboring $^{204}\text{Po}^*$ and other radioactive CN such as $^{220}\text{Th}^*$.

For g.s. to g.s. decay of $^{202}\text{Po}^*$, formed via $^{48}\text{Ca} + ^{154}\text{Gd}$ reaction, involving deformed rare-earth lanthanide target, the only observed $4n$ decay channel is shown to require a considerable quasifissionlike nCN contribution. On the other hand, our DCM calculations match the experimental data for $3n$ and $5n$ metastable-state decay channels, i.e., from g.s. of $^{202}\text{Po}^*$ to m.s. states ^{199m}Po and ^{197m}Po nuclei, as pure CN decays, meaning thereby that $3n$ and $5n$ metastable states are best fitted with zero nCN contribution. Interestingly, both the observed g.s. to g.s. and g.s. to m.s. decays are found to occur at one constant neck length $\Delta R = 2.45 \pm 0.20$ fm, a much larger value compared to other unobserved decays. Such a result, in particular for g.s. to m.s. decay, is shown here for the first time.

Furthermore, the variation of CN formation and survival probabilities P_{CN} and P_{surv} with excitation energy E_{CN}^* for the decay of radioactive $^{202}\text{Po}^*$ is found to fit with the systematic of other radioactive compound systems studied within the DCM, giving strength to our predictions, in particular, the predicted fusion-fission (σ_{ff}) cross sections and σ_{qf} predicted for the g.s. to g.s. decay of $^{202}\text{Po}^*$. Thus, the two different kinds of decays of the same compound nucleus are shown to be governed by different CN decay processes with g.s. to g.s. decay of $^{202}\text{Po}^*$ requiring qf-like, nCN contribution, and the g.s. to m.s. decay of $^{202}\text{Po}^*$ being a pure CN decay.

ACKNOWLEDGMENT

Work supported by Department of Science and Technology (DST), New Delhi, India, in the form of SERB major research project F. No. EMR/2016/001131.

- [1] T. S. Oganessian, in *Heavy Elements and Related New Phenomena*, Vols. I and II, edited by W. Greiner and R. K. Gupta (World Scientific, Singapore, 1999).
- [2] M. G. Itkis *et al.*, *J. Nucl. Radiochem. Sci.* **3**, 57 (2002).
- [3] D. Vermeulen *et al.*, *Z. Phys. A* **318**, 157 (1984).

- [4] K. Kim, Y. Kim, A. K. Nasirov, G. Mandaglio, and G. Giardina, *Phys. Rev. C* **91**, 064608 (2015).
- [5] C. C. Sahn, H. G. Clerc, K. H. Schmidt, W. Reisdorf, P. Armbruster, F. P. Hessberger, J. G. Keller, G. Münzenberg, and D. Vermeulen, *Nucl. Phys. A* **441**, 316 (1985).

- [6] R. N. Sagaidak, G. N. Kniajeva, I. M. Itkis, M. G. Itkis, N. A. Kondratiev, E. M. Kozulin, I. V. Pokrovsky, A. I. Svirikhin, V. M. Voskressensky, A. V. Yeremin, L. Corradi, A. Gadea, A. Latina, A. M. Stefanini, S. Szilner, M. Trotta, A. M. Vinodkumar, S. Beghini, G. Montagnoli, F. Scarlassara, D. Ackermann, F. Hanappe, N. Rowley, and L. Stuttge, *Phys. Rev. C* **68**, 014603 (2003).
- [7] G. N. Knyazheva, E. M. Kozulin, R. N. Sagaidak, A. Yu. Chizhov, M. G. Itkis, N. A. Kondratiev, V. M. Voskressensky, A. M. Stefanini, B. R. Behera, L. Corradi, E. Fioretto, A. Gadea, A. Latina, S. Szilner, M. Trotta, S. Beghini, G. Montagnoli, F. Scarlassara, F. Haas, N. Rowley, P. R. S. Gomes, and A. Szanto de Toledo, *Phys. Rev. C* **75**, 064602 (2007).
- [8] D. A. Mayorov, T. A. Werke, M. C. Alfonso, M. E. Bennett, and C. M. Folden, III, *Phys. Rev. C* **90**, 024602 (2014).
- [9] D. J. Hinde, M. Dasgupta, and A. Mukherjee, *Phys. Rev. Lett.* **89**, 282701 (2002).
- [10] Hemdeep, S. Chopra, A. Kaur, and R. K. Gupta, *Phys. Rev. C* **95**, 014609 (2017).
- [11] R. Rafiei, R. G. Thomas, D. J. Hinde, M. Dasgupta, C. R. Morton, L. R. Gasques, M. L. Brown, and M. D. Rodriguez, *Phys. Rev. C* **77**, 024606 (2008).
- [12] <http://www.nndc.bnl.gov>.
- [13] R. K. Gupta, S. K. Arun, R. Kumar, and Niyti, *Int. Rev. Phys. (IREPHY)* **2**, 369 (2008).
- [14] R. K. Gupta, in *Clusters in Nuclei*, Lecture Notes in Physics 818, edited by C. Beck, Vol. I (Springer-Verlag, Berlin, 2010), p. 223, and earlier references therein.
- [15] R. K. Gupta, Review article in *Nuclear Particle Correlations and Cluster Physics*, edited by W.-U. Schröder (World Scientific, Singapore, 2017), p. 471.
- [16] R. K. Gupta, M. Balasubramaniam, R. Kumar, N. Singh, M. Manhas, and W. Greiner, *J. Phys. G: Nucl. Part. Phys.* **31**, 631 (2005).
- [17] M. Kaur and M. K. Sharma, *Phys. Rev. C* **85**, 054605 (2012).
- [18] A. Săndulescu, R. K. Gupta, W. Scheid, and W. Greiner, *Phys. Lett. B* **60**, 225 (1976).
- [19] R. K. Gupta, A. Săndulescu, and W. Greiner, *Phys. Lett. B* **67**, 257 (1977).
- [20] G. Adamian, N. Antonenko, and W. Scheid, in *Clusters in Nuclei*, edited by C. Beck, Lecture Notes in Physics 848 (Springer, Heidelberg, 2012), Vol. 2, p.165.
- [21] G. Mandaglio, G. Giardina, A. K. Nasirov, and A. Sobczewski, *Phys. Rev. C* **86**, 064607 (2012).
- [22] W. J. Świątecki, K. Siwek-Wilczyńska, and J. Wilczyński, *Phys. Rev. C* **71**, 014602 (2005).
- [23] K. Siwek-Wilczyńska *et al.*, *Int. J. Mod. Phys. E* **17**, 12 (2008).
- [24] R. Vandenbosch and J. Huizenga, *Nuclear Fission* (Academic, New York, 1973), p. 227.
- [25] P. Kaushal, S. Chopra, Hemdeep, and R. K. Gupta, Proceedings DAE-BRNS Symposium on Nucl. Phys. **62**, 476 (2017), available at <http://sympnp.org/proceedings/62/B58.pdf>.
- [26] H. Kröger and W. Scheid, *J. Phys. G* **6**, L85 (1980).
- [27] W. Myers and W. J. Świątecki, *Nucl. Phys.* **81**, 1 (1966).
- [28] A. S. Jensen and J. Damgaard, *Nucl. Phys. A* **203**, 578 (1973).
- [29] N. J. Davidson, S. S. Hsiao, J. Markram, H. G. Miller, and Y. Tzeng, *Nucl. Phys. A* **570**, 61c (1994).
- [30] R. K. Gupta, R. Kumar, N. K. Dhiman, M. Balasubramaniam, W. Scheid, and C. Beck, *Phys. Rev. C* **68**, 014610 (2003).
- [31] M. Balasubramaniam, R. Kumar, R. K. Gupta, C. Beck, and W. Scheid, *J. Phys. G: Nucl. Part. Phys.* **29**, 2703 (2003).
- [32] B. B. Singh, M. K. Sharma, and R. K. Gupta, *Phys. Rev. C* **77**, 054613 (2008).
- [33] G. Audi, A. H. Wapstra, and C. Thibault, *Nucl. Phys. A* **729**, 337 (2003).
- [34] P. Möller, J. R. Nix, W. D. Myers, and W. J. Świątecki, *At. Data Nucl. Data Tables* **59**, 185 (1995).
- [35] R. K. Gupta, in *Proceedings of the 5th International Conference on Nuclear Reaction Mechanisms, Varenna, Italy*, edited by E. Gadioli (Ricerca Scientifica Educazione Permanente, Italy, 1988), p. 416.
- [36] S. S. Malik and R. K. Gupta, *Phys. Rev. C* **39**, 1992 (1989).
- [37] R. K. Gupta, M. Horio, A. Săndulescu, M. Greiner, and W. Scheid, *J. Phys. G: Nucl. Part. Phys.* **19**, 2063 (1993).
- [38] H. S. Khosla, S. S. Malik, and R. K. Gupta, *Nucl. Phys. A* **513**, 115 (1990).
- [39] S. Kumar and R. K. Gupta, *Phys. Rev. C* **55**, 218 (1997).
- [40] R. K. Gupta, S. Kumar, and W. Scheid, *Int. J. Mod. Phys. E* **6**, 259 (1997).
- [41] T. Matsuse, C. Beck, R. Nouicer, and D. Mahboub, *Phys. Rev. C* **55**, 1380 (1997).
- [42] S. J. Sanders, A. Szanto de Toledo, and C. Beck, *Phys. Rep.* **311**, 487 (1999).
- [43] S. J. Sanders, *Phys. Rev. C* **44**, 2676 (1991).
- [44] S. J. Sanders, D. G. Kovar, B. B. Back, C. Beck, D. J. Henderson, R. V. F. Janssens, T. F. Wang, and B. D. Wilkins, *Phys. Rev. C* **40**, 2091 (1989); S. J. Sanders, D. G. Kovar, B. B. Back, C. Beck, B. K. Dichter, D. Henderson, R. V. F. Janssens, J. G. Keller, S. Kaufman, T.-F. Wang, B. Wilkins, and F. Videbaek, *Phys. Rev. Lett.* **59**, 2856 (1987).
- [45] G. Royer and J. Mignen, *J. Phys. G: Nucl. Part. Phys.* **18**, 1781 (1992).
- [46] A. Kaur, S. Chopra, and R. K. Gupta, *Phys. Rev. C* **90**, 024619 (2014).
- [47] S. Chopra, A. Kaur, and R. K. Gupta, *Phys. Rev. C* **91**, 034613 (2015).